Structural and magnetic properties of amorphous Fe/Zr multilayers

1997 J. Phys.: Condens. Matter 9 10603

(http://iopscience.iop.org/0953-8984/9/48/006)

J. Phys.: Condens. Matter **9** (1997) 10603–10614. Printed in the UK PII: S0953-8984(97)83894-5

Structural and magnetic properties of amorphous Fe/Zr multilayers

F J Castaño†, T Stobiecki‡, M R J Gibbs†, M Czapkiewicz‡,
M Kopcewicz§, V Gacem†, J Speakman†, N Cowlam† and H J Blythe†

† Department of Physics, University of Sheffield, Sheffield S3 7RH, UK

‡ Department of Electronics, University of Mining and Metallurgy, Al. Mickiewicza 30, 30-059 Krakow, Poland

§ Institute of Electronic Materials Technology, Wolczynska 133, 01-919 Warszawa, Poland

Received 1 May 1997, in final form 10 July 1997

Abstract. The structure and magnetic properties of rf-sputtered Fe/Zr multilayers with ultrathin layer thicknesses, in as-deposited and annealed states, have been studied using x-ray diffraction, low- angle x-ray reflectometry, conversion electron Mössbauer spectroscopy and low-temperature magnetometry. The thickness ratio (d_{Fe}/d_{Zr}) of the analysed multilayers was 0.5 and the values of the bilayer thickness ($d_{Fe} + d_{Zr}$) was varied from 9 Å to 75 Å, maintaining constant the total thickness of the samples by controlling the number of bilayers. The results obtained show that, during sputter deposition, Fe layers with thicknesses below 20 Å are alloyed forming an amorphous Fe_2Zr phase. Those multilayers with nominal Fe layer thickness below 20 Å are composed of layers of this amorphous phase, behave as a ferromagnet below the Curie temperature (138 ± 0.5 K), and the spin structure shows a low-temperature asperomagnetic ground state with a reduced canting of the spin structure as compared with homogeneous Fe_2Zr amorphous thin films. The structural relaxation during annealing indicates that an homogeneous Fe–Zr amorphous alloy can be produced after annealing these Fe/Zr multilayer structures.

1. Introduction

Metallic multilayers composed of alternating layers of Fe and other transition metals exhibit a range of novel magnetic properties, such as giant magnetoresistance and oscillating interlayer coupling (e.g. Fe/Cr [1] and Fe/Nb [2]). These properties can be manipulated by changing such parameters as the bilayer thickness, the topography of the interfaces, the layer crystalline structure or the preparation conditions. Technological devices using sputtered magnetic multilayers with ultrathin layers are increasingly needed and the nature of the interfaces in these structures appears to be critical. As a result, fundamental studies relating the structure and the magnetic properties of Fe-based multilayers with ultrathin layer thicknesses are of increasing interest.

Recently it has been reported that in Fe/early transition metal (ETM) multilayer structures (e.g. ETM = Zr [3], Y [4], Ti [5], Mo [6], Hf [7]), a transition from a polycrystalline to an amorphous phase occurs via a solid state reaction (SSR) during sputter deposition, on decreasing the layer thicknesses of both Fe and the ETM below a critical value, d_c, which is different for each element. In polycrystalline Fe/ETM multilayers ($d > d_c$), the existence of an amorphous Fe–ETM alloy region, between the crystalline layers and in the grain boundaries, has been supported by conversion electron Mössbauer spectroscopy (CEMS), x-ray diffraction (XRD), electrical conductivity and room-temperature magnetic measurements (Fe/Ti [8], Fe/Zr [9]).

0953-8984/97/4810603+12$19.50

The values of the heat of formation, ΔH, for Fe–ETM amorphous phases appear to be negative [10], so that an alloy with Fe–ETM bonds can be expected to appear in the interfaces between layers. For this reason the magnetic behaviour of amorphous Fe/ETM multilayers should arise from a structure with predominant Fe–Fe or Fe–ETM metallic bonds depending on the thickness of the layers and interface regions. Above the critical thickness the Fe layers are in the well known ferromagnetic bcc state (α-Fe), and the layers formed of the hcp ETM elements are in a paramagnetic state.

In the case of amorphous Fe/ETM multilayers with ultrathin layer thicknesses, the structural origin of the magnetic state is not fully understood [11] and the atomic dimensions of the layers makes a direct observation of the structure very difficult. Two growth models have been assumed in order to interpret the structural and magnetic results for amorphous multilayers.

The first growth model [12–16] assumes a planar growth of the amorphous phases corresponding to each element of the multilayer with sharp interfaces between the layers. This picture represents a pure interface effect and is believed to arise from an extreme mismatch between the lattice parameters of the crystalline phases formed in these multilayer structures for layer thicknesses above d_c. This argument is weak, since in general the interatomic distances in a crystalline phase are different to those in the corresponding amorphous phase. If this model were to simulate the real structure, these ultrathin multilayers would provide a production route for pure amorphous Fe (α-Fe).

The second growth model [17, 18] suggests that for Fe/ETM multilayers an amorphous Fe–ETM phase is formed during sputter deposition in the plane between layers as well as in the grain boundaries. This picture suggests that the magnetic behaviour of amorphous Fe/ETM multilayers will have a contribution from the amorphous Fe–ETM phase formed during sputter deposition. Since the effect of this on the magnetic behaviour is not clear, it is important to study and compare the magnetic behaviour of sputtered amorphous Fe/ETM multilayer structures and sputtered $Fe_x(ETM)_{100-x}$ amorphous alloys.

Fe/Zr is an interesting multilayer system for the exploration of structural properties since there is an extreme mismatch between the lattice parameters of bcc Fe and the hcp Zr. The magnetic properties of amorphous Fe–Zr alloys have been studied using samples obtained by methods such as mechanical alloying [19], sputter deposition [20], liquid quenching [21] and annealing or irradiation of Fe/Zr multilayers [22–24]. On the other hand, brief studies of the magnetic properties of sputtered Fe/Zr multilayer structures in an as-deposited amorphous state have been undertaken and seemed inconclusive [14]. The Curie temperatures of ferromagnetic Fe–Zr amorphous alloys are well below room temperature (for a review see [25]), so that their study needs low-temperature magnetometry techniques.

The Fe–Zr system appears to be particularly convenient to study amorphous phase formation by room-temperature CEMS since all amorphous Fe–Zr phases reveal a quadrupole-split doublet, distinct from the hyperfine structure of α-Fe. In the same way the difference in the x-ray scattering length densities of Fe (62.1×10^{-6} Å^{-2}) and Zr (48.3×10^{-6} Å^{-2}) [26] makes x-ray reflectometry (XRR) an ideal method to examine Fe/Zr multilayer samples.

In this paper we will present a detailed structural and magnetic characterization of Fe/Zr layered structures, with Fe layer thicknesses around d_c, using XRD, XRR, room-temperature CEMS and low-temperature magnetic measurements of as-deposited and annealed Fe/Zr multilayers with ultrathin Fe layer thicknesses. The magnetic properties of these amorphous Fe/Zr multilayers will be compared with those of sputtered Fe_xZr_{100-x} amorphous alloys [25].

2. Experimental details

Fe/Zr multilayers were deposited from iron and zirconium targets by rf-sputtering, onto water-cooled glass substrates, in an Ar atmosphere. The pressure during sputtering was 1×10^{-2} mbar of argon gas and the deposition rates, as determined from calibration growths, were 4.6 nm min^{-1} and 6 nm min^{-1} for iron and zirconium respectively. The nominal thickness ratios ($\beta = d_{Fe}/d_{Zr}$) of the three samples investigated were 3/6 Å, 13/26 Å and 25/50 Å, respectively. It must be emphasized that sputtered layers with very low thicknesses may well not be continuous due to island growth. In order to discuss the results in a coherent manner, the total thickness of the samples was kept constant (≈2400 Å) by controlling the number of bilayers. The total thickness of the samples was checked by step profiling.

XRD measurements were performed on all three samples using Bragg–Brentano geometry and Co Kα radiation. An opportunity arose to examine the layered structure of samples 3/6 Å and 13/26 Å by XRR measurements which were performed with a horizontal HUBER diffractometer which was mounted on a Philips PW1130 generator with Cu Kα radiation. The CEMS measurements of the three samples were performed at room temperature with a conventional constant-acceleration computer-controlled Mössbauer spectrometer using an He–6% CH_4 gas flow electron counter. The Mössbauer spectral parameters were obtained by fitting Lorentzian line shapes to the experimental data by the least-squares method. The quadrupole splitting distributions were obtained by using the constrained Hesse–Rübartsch method [27, 28].

Magnetic measurements were made in fields up to 5 T and at temperatures from 5 K to 300 K using a Quantum Design MPMS SQUID magnetometer. The magnetic field values could be set to an accuracy of $\pm 10^{-6}$ T and the temperatures to within $\pm 10^{-2}$ K. Two types of magnetic measurement were made: (a) measurements of hysteresis loops in fields covering the range -5 T $\leqslant \mu_0 H \leqslant 5$ T and over a wide range of temperatures, (b) zero-field cooled/field cooled (ZFC/FC) measurements in applied fields within the range 1 mT $\leqslant \mu_0 H \leqslant 50$ mT (to perform these measurements the superconducting coil of the SQUID was quenched to eliminate any trapped flux). The coercivity and saturation magnetic moments could be determined from the hysteresis loop measurements. Accurate values of the Curie temperatures, T_C, were obtained from Arrott–Noakes plots [29] (some of the conclusions derived from this calculation will be published elsewhere). The samples were first measured as described above and then the film was removed from the substrate by dissolving it in acid. To correct the above magnetic measurements for the diamagnetic contribution of the substrate, the remaining substrate was then re-measured using the same programme as previously used for the whole sample.

3. Results

3.1. Structure

Figure 1 shows XRD measurements of the three samples corrected for the diffracted intensity from the substrate, presented over the range $1.75 \leqslant Q \leqslant 3.5$ Å^{-1}. The pattern for the 3/6 Å sample has a broad halo, while for the 13/26 Å sample a single maximum at $Q \approx 2.3$ Å^{-1} is observed, which can be identified as a Bragg peak from the zirconium in the pattern of the 25/50 Å sample. The iron (110) Bragg peak is observed at $Q \approx 3.1$ Å^{-1} only for this latter sample.

These diffraction patterns can be understood in terms of the Scherrer equation [30]

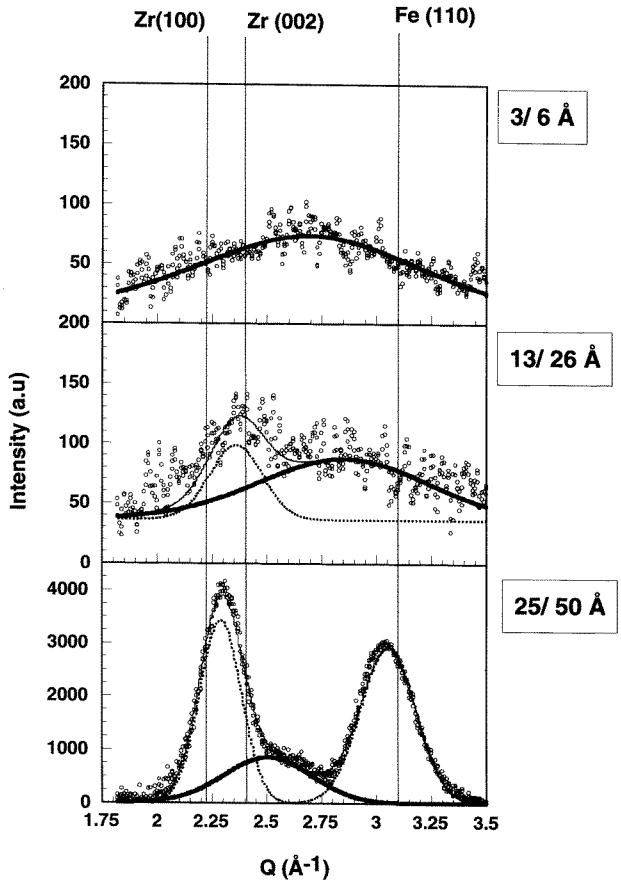

Figure 1. XRD measurements and fits of Fe/Zr multilayers with ultrathin layer thicknesses. Open circles correspond to the experimental data. Solid circle lines represent the amorphous fraction, dashed lines the amount of hcp Zr and bcc Fe and solid lines are the sum of the above fitted curves.

which gives the Bragg peak broadening, δQ, in terms of the crystal size D. It can be assumed that the layers in these sputter samples have a high density of grain boundaries so that to a first approximation the grain size may be equivalent to the layer thickness. Application of the Scherrer equation then gives the values of the peak breadth for the three samples shown in table 1.

We may conclude that the diffraction pattern for the 3/6 Å sample alone (in the absence of the CEMS data discussed below) does not allow a distinction to be made between an amorphous or microcrystalline phase. The peak broadening in the diffraction patterns of the 13/26 Å and 25/50 Å is consistent with the particle size broadening and these data (over a restricted range of Q values) do not allow a distinction between particle size broadening, strain and alloying effects to be made.

If an amorphous phase is present, the relative fractions of the bcc Fe, hcp Zr and amorphous Fe–Zr phases can be estimated from the integrated intensity of the XRD lines [31]. A pseudo-Voigt shape for the diffraction peaks was used in the calculations (the fittings are shown in figure 1). Reasonable values of the volume fractions can obtained

Table 1.

Sample	Layer element	Nominal layer thickness (Å)	δQ (Å^{-1})
3/6 Å	Fe based	3	2.1
	Zr based	6	1.0
13/26 Å	Fe based	13	0.48
	Zr based	26	0.24
25/50 Å	Fe based	25	0.25
	Zr based	50	0.13

since the calculated average atomic composition of the analysed samples is $Fe_{50}Zr_{50}$ (this can be obtained using both the fact that for all the samples $\beta = 0.5$ and the knowledge of the relative atomic masses and densities of bcc Fe and hcp Zr). It was only possible to estimate the relative increment of the amorphous phase in the absence of an absolute intensity measurement. According to the these calculations the sample 13/26 Å is composed of 15% of hcp Zr ($D_{Zr} = 22$ Å) and 85% of amorphous phase and sample 25/50 Å is formed by 19.5% of bcc Fe ($D_{Fe} = 22$ Å), 36.8% of hcp Zr ($D_{Zr} = 24$ Å) and 43.7% of amorphous phase.

Another concern of the present work is determining the structural and magnetic state of as-deposited Fe layers in Fe/Zr multilayers. For this reason, the layered structure of samples 3/6 Å and 13/26 Å was analysed by XRR measurements (figure 2). The bilayer thicknesses, as calculated from the position of the Bragg peaks, which are given in table 2, agree within a few per cent with the nominal bilayer thickness estimated from the deposition rates.

The reflectivity profile of the sample 3/6 Å displays a Fresnel fall-off which decays as Q^{-4}; however the interference fringes whose positions correspond to the total thickness of the sample are not visible [32], perhaps because the upper surface of the sample is rough. A weak Bragg peak at $Q = 0.714$ Å^{-1} is observed, from which the layer period can be deduced. On the other hand, up to three orders of Bragg peak can be resolved in the reflectivity profile of the 13/26 Å sample, which provide firm evidence for the bilayer spacing not far from the nominal one.

The above XRD and XRR measurements for the 3/6 Å sample can be interpreted as showing a modulated structure (from the weak XRR peak whose position agrees with the nominal thickness) composed of an Fe-based and a Zr-based amorphous phase (see later, section 3.2, for further support). In the same way, the 13/26 Å sample can be ascribed to a modulated structure composed of both an Fe-based amorphous and a crystalline hcp Zr phase.

In order to study the nature of the Fe-based phases in the analysed samples, fitting and simulation of these data (shown in figure 2) were made by using the Born approximation. This model neglects high-order reflections in the multilayer structure [32]. The fitting parameters were: the layer thicknesses, the roughness of the interfaces, and the critical wave vector (Q_c) which is related to the electronic density. This approximation yields good fits for experimental data with $Q > Q_c$. The results obtained from these fits are shown in table 2.

The values of the interface roughness agree with those reported earlier on DC-sputtered and electron-beam-evaporated amorphous Fe/Zr multilayer samples [3]. Several conclusions can be drawn from table 2. (a) The values of the electronic density obtained for the Fe-based layers are lower than that of α-Fe (60.13×10^{-6} Å^{-2}) [26]. It can be inferred from this

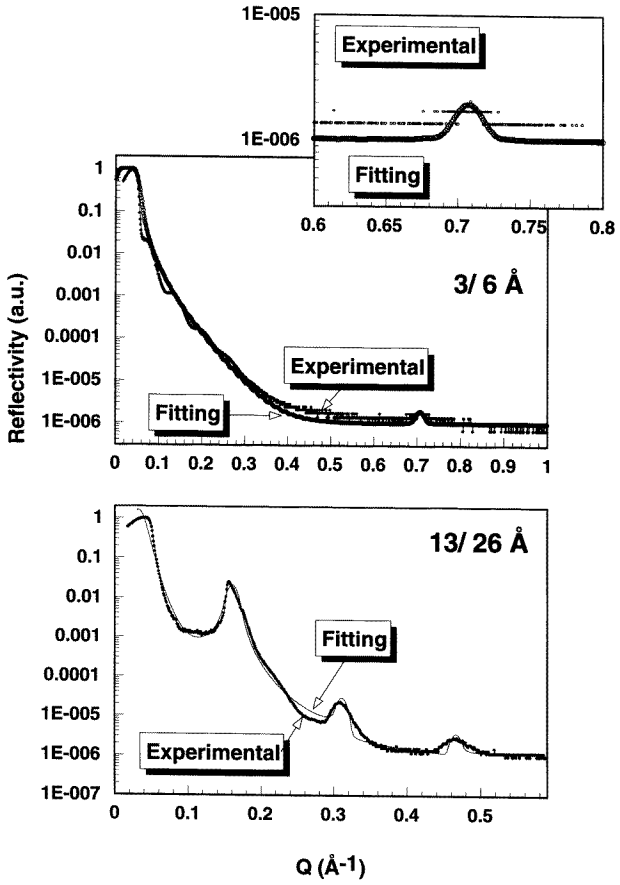

Figure 2. XRR measurements (scatter line) and fits for Fe/Zr multilayer samples 3/6 Å and 13/26 Å.

Table 2.

Sample	Bilayer thickness (Å)	Layer label	Layer thickness (Å)	Electronic density ($\times 10^{-6}$ Å^{-2})	Interface roughness (Å)
3/6 Å	8.9	Fe based	3	49.74	2.5
		Zr based	5.9	53.79	3
13/26 Å	41	Fe based	18.4	47.7	4.5
		Zr based	22.6	42.1	4.5

that the Fe-based layers are alloyed. (b) On the other hand, the increase of the Fe-based layer thickness in sample 13/26 Å, as compared with nominal Fe layer thickness, can also be interpreted as alloying taking place during sputter deposition. This supports the point made in the introduction that the planar growth model [11–16] is not probable.

The Mössbauer spectra, as well as the distributions of the quadrupole splitting, $P(\mathrm{QS})$, of sample 3/6 Å, 13/26 Å and 25/50 Å are shown in figure 3. To obtain these results the

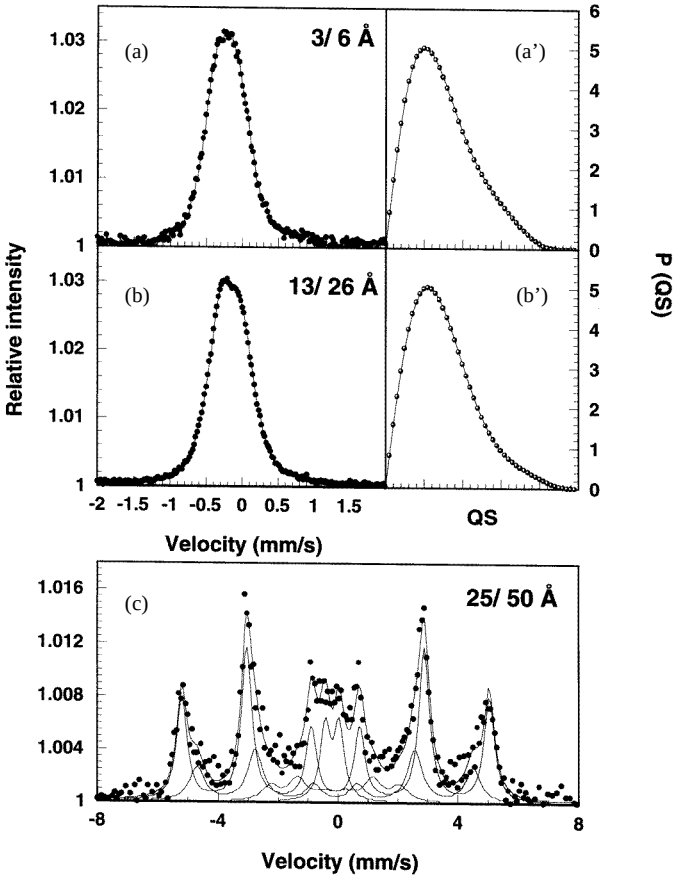

Figure 3. CEMS spectra for samples 3/6 Å (a), 13/26 Å (b) and 25/50 Å (c), as well as the $P(\mathrm{QS})$ distributions for samples 3/6 Å (a') and 13/26 Å (b').

spectra were measured in a reduced velocity range. The spectra of the 25/50 Å sample shows a hyperfine structure characteristic of α-Fe.

On the other hand, the $P(\mathrm{QS})$ distributions for samples 3/6 Å and 13/26 Å appear to be wider than those reported for Fe_xZr_{100-x} amorphous alloys [24] and show a bell-like shape without any distinct structure, suggesting that the composition of the magnetic amorphous phases formed during deposition in these samples is homogeneous and similar. The values of the average quadrupole splitting (QS) are 0.32 ± 0.01 mm s^{-1} and 0.33 ± 0.01 mm s^{-1}, for samples 3/6 Å and 13/26 Å, respectively. Comparing these results of the QS with those which we have reported earlier [24], the magnetic phase formed from the SSR of the sputter-deposited Fe layers in both samples can be regarded as an amorphous Fe_2Zr phase. This is also supported by the difference between the present values of the QS and that reported for nominal amorphous Fe (0.25 mm s^{-1}) [33].

3.2. Magnetic properties

Thermo-magnetization measurements with different applied fields for the three analysed samples are shown in figure 4.

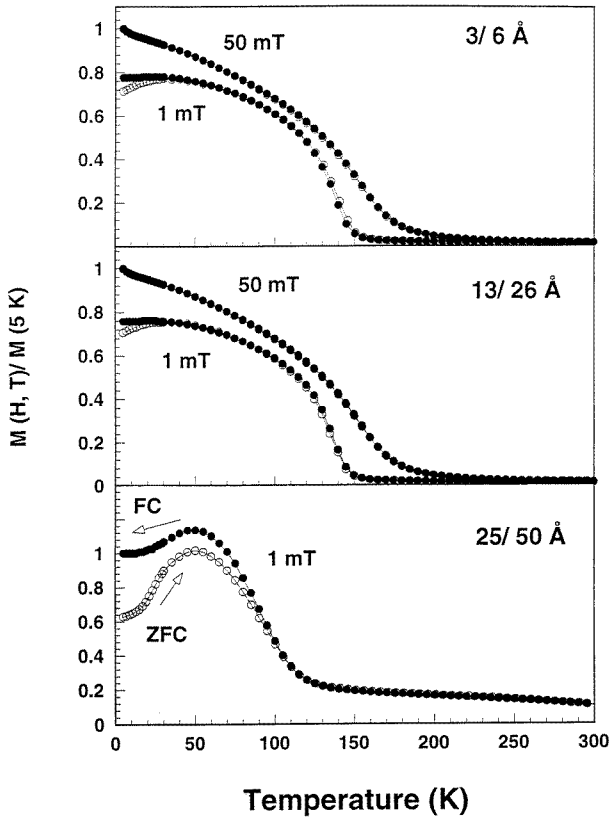

Figure 4. Temperature dependence of the normalized magnetization of Fe/Zr multilayers with ultrathin layer thicknesses for different applied fields. ZFC measurements are represented by open symbols and FC by solid symbols.

Sample 25/50 Å is slightly ferromagnetic at room temperature due to the existence of small crystals of α-Fe, as deduced from the XRD measurements. These small crystallites are responsible for the low temperature superparamagnetic behaviour of this sample shown in figure 4. The blocking temperature is around 50 K which agrees with the temperature where the coercivity disappears. This measurement was repeated using different parts of the same sample and the values of the blocking temperature (which is related to the crystal sizes) were the same, indicating negligible variation of the Fe layer thickness through the sample.

The thermo-magnetic behaviour of samples 3/6 Å and 13/26 Å are similar. It is clear from figure 4 that both samples are paramagnetic in the temperature range 150–300 K, showing a sharp Curie temperature evident in the low-field measurements. The Curie temperature for both samples is (138 ± 0.5) K, as calculated from Arrott–Noakes plots. This value of T_C corresponds approximately to an $Fe_{60}Zr_{40}$ amorphous phase [25] which is in good agreement (within the error of the extrapolation method used to obtain T_C) with an amorphous Fe_2Zr phase, hence both samples, prepared with a calculated average atomic composition of $Fe_{50}Zr_{50}$, transform to a more stable Fe_2Zr amorphous phase. The fact that the Curie temperature in the low-field range is sharp indicates that only one magnetic phase contributes to the magnetic behaviour.

In the low field range the magnetization shows an irreversible thermal behaviour below a certain temperature T_{xy} which depends on the intensity of the applied field. The splitting between the ZFC and the FC measurements can be interpreted as evidence for the existence of a non-collinear magnetic behaviour as we have discussed previously [25]. The disappearance of coercivity at low temperatures is not related to the temperatures where this splitting occurs giving evidence [34] for the asperomagnetic behaviour of these two samples. The high-field susceptibility appears to be low as compared with homogeneous Fe_2Zr amorphous alloys [25, 35] and both samples are saturated at fields around 1 T.

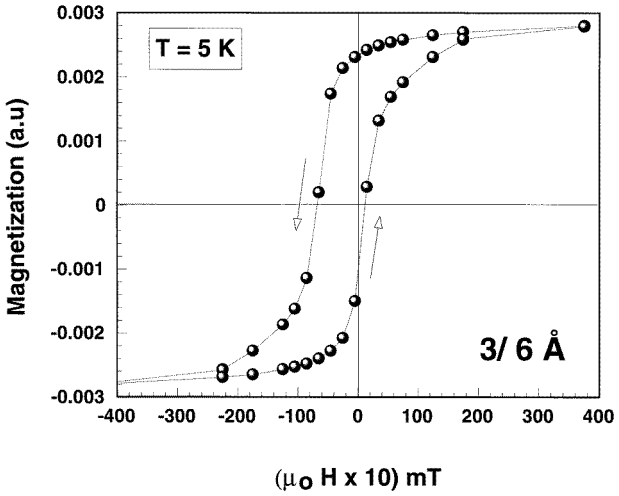

Figure 5. Displaced hysteresis loop at 5 K when sample 3/6 Å was cooled down in a negative field of −100 mT (solid lines are just a guide to the eye).

Figure 5 shows a displaced hysteresis loop at 5 K when sample 3/6 Å was cooled down in a negative field of −100 mT. This behaviour is a characteristic feature of spin-glass-like amorphous systems [36]. With all the above, the low-temperature magnetic state of samples 3/6 Å and 13/26 Å can be regarded as a correlated spin glass or asperomagnetic. The values of the magnetic moment (μ_{Fe}) at 5 K for samples 3/6 Å and 13/26 Å are 0.96 μ_B and 0.95 μ_B, which also correspond to an amorphous Fe_2Zr phase [25].

In order to understand how the spin structure relaxes during annealing, sample 25/50 Å was annealed at different temperatures for 2 hours in a conventional low-vacuum annealing system. Figure 6 show the FC measurements in an applied field of 1 mT for the different annealing stages investigated.

Due to the SSR during annealing, the α-Fe grains present in this sample (as deduced from the XRD measurements) start to disappear and the constant contribution of this phase, above the Curie temperature, disappears after annealing the sample at 500 K for 2 hours. Around the Curie temperature the constant contribution of the existing α-Fe phase can be subtracted and the value of the Curie temperature was estimated. These values can be associated with the existence of an Fe–Zr amorphous phase with different composition for each annealing stage. The Curie temperature of the amorphous phase in the sample annealed at 500 K is 140 K, which is in good agreement with an amorphous Fe_2Zr phase [25]. These results agree with previously reported data [37] on the SSR of Fe/Zr multilayers during annealing.

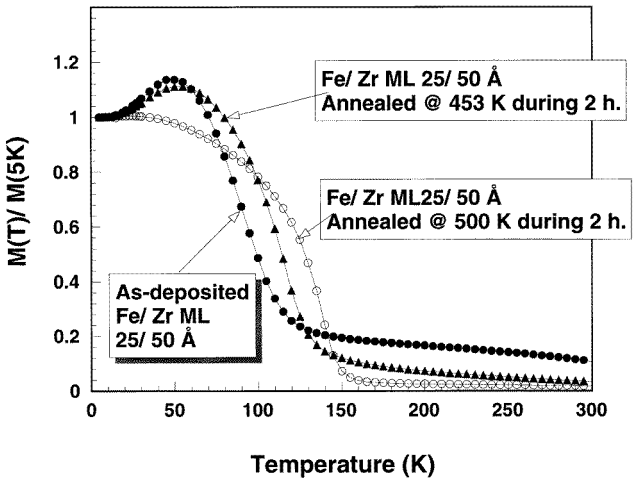

Figure 6. FC measurements of different annealing stages of sample 25/50 Å in an applied field of 1 mT.

4. Discussion

The as-deposited samples reveal the three different stages of the SSR that occurs during sputtering deposition in the Fe/Zr multilayer system. We have shown that there is an amorphous Fe_2Zr alloy formed during sputtering deposition and hence the present results can only be understood according to the second growth model described in the introduction. This model predicts a local maximum in the free energy curve for an amorphous alloy with the same average atomic composition as the multilayers that we have analysed [37]. This suggests that amorphous phases Fe_2Zr and $FeZr_2$ are more stable and therefore more likely to appear, which agrees with the present results.

According to the above model and the present results, sample 3/6 Å can be regarded as a modulated structure composed of two amorphous Fe–Zr phases. The Fe-rich amorphous phase formed in sample 3/6 Å, which is responsible for the low-temperature magnetic response of these multilayers, appears to be similar to that formed from the as-deposited Fe layers in sample 13/26 Å. The magnetic results can only be understood with such a model since amorphous Fe–Zr alloys with a composition ratio of 1:2 are diamagnetic [25]. This Fe-poor amorphous phase that would appear in sample 3/6 Å will not contribute to the magnetic behaviour and in this way the thermo-magnetic behaviour of samples 3/6 Å and 13/26 Å in a small applied field should be the same. In the same way the asperomagnetic state that we have previously reported in the Fe–Zr amorphous alloy system [25] also agrees with the state inferred for Fe/Zr amorphous multilayers in the present work.

The constraints imposed by the modulated structure on the spin structure are probably responsible for the reduction in the high-field susceptibility (homogeneous amorphous Fe–Zr alloys cannot be saturated with fields of 5 T [35]). Our previous CEMS measurements in polycrystalline Fe/Zr multilayers [24] show an in-plane direction of the magnetic moments, so one could infer that the canting of the magnetic moments in the Fe_2Zr amorphous layers may be reduced as compared with intrinsic canting of homogeneous rf-sputtered amorphous Fe_2Zr alloy, and this indeed appears to be the case. There has been a long debate about the magnetic properties of pure amorphous Fe [38]. The possibility of producing this phase

in amorphous multilayers structures has generated a large amount of work studying the magnetic properties of different Fe/ETM amorphous multilayers with ultrathin Fe layers. If a model of sharp interfaces between the amorphous layers was to be reasonable no alloying should take place during deposition and this is very difficult to support from the results presented here. Our results in the Fe/Zr Ml system show that the amorphous phase responsible for the magnetic results when the Fe layers have thicknesses below 20 Å can be regarded as an Fe_2Zr amorphous alloy.

5. Summary and conclusions

We have shown that multilayer systems with alternately stacked Zr and Fe layers and with good periodicity may be grown by rf sputtering with ultrathin Fe deposited layers. The Fe layers first grow in an amorphous Fe–Zr phase up to a critical thickness around 20 Å, and then change to a bcc crystalline state. Our results show that samples with Fe layers below the critical thickness can be described as layered structure composed of layers of Fe_2Zr amorphous alloy. These samples are ferromagnetic with a Curie temperature of 138 K and a low-temperature asperomagnetic ground state. The effect of the modulated structure is to reduce the magnetic moment canting in multilayer samples as compared with Fe–Zr homogeneous amorphous magnetic state.

Acknowledgments

This work was supported by grant No 8 T11B 05811 from the Polish Committee for Scientific Research. We also thank Professor A Gibaud for his assistance with the XRR measurements.

References

[1] Sato N 1986 *J. Appl. Phys.* **59** 2514
[2] Rehm C, Klose F, Nagengast D, Pietzak B, Maletta H and Weidinger A 1996 *Physica* B **221** 377
[3] Clemens B M and Williamson D L 1988 *Mater. Res. Soc. Symp. Proc.* vol 103 (Pittsburgh, PA: Materials Research Society) p 159
[4] Badia F, Ferrater C, Martinez B, Lousa A and Tejada J 1991 *J. Magn. Magn. Mater.* **93** 429
[5] Czapkiewicz M, Stobiecki T and Kopcewicz M 1996 *J. Magn. Magn. Mater.* **160** 357
[6] Cu F Z, Wang Y, Cui H, Li W Z and Fan Y D 1994 *J. Phys. D: Appl. Phys.* **27** 2246
[7] Shringi S N, Piramanayagam S N, Prasad S, Venkatramani N, Patni M J, Krishnan R and Tessier M 1993 *J. Appl. Phys.* **73** 6438
[8] Kopcewicz M, Stobiecki T, Czapkiewicz M and Grabias A 1997 *J. Phys.: Condens. Matter* **9** 103
[9] Stobiecki T, Czapkiewicz M, Kopcewicz M, Zuberek R and Castaño F J *10th Int. Conf. on Thin Films (Salamanca, 1996)* at press
[10] Boom R, Deboer F R, Niessen A K and Miedema A R 1983 *Physica* B&C **115** 285
[11] Samwer K 1988 *Phys. Rep.* **161** 1
[12] Handschuh S, Landes J, Köbler U, Sauer Ch, Kisters G, Fuss A and Zinn W 1993 *J. Magn. Magn. Mater.* **119** 254
[13] Dubowik J, Stobiecki F, Rohrmann H and Roll K 1996 *J. Magn. Magn. Mater.* **152** 201
[14] Dubowik J 1995 *J. Magn. Magn. Mater.* **140–144** 531
[15] Clemens B M 1988 *J. Less-Common Met.* **140** 57
[16] Geisler H, Herr U, Lorentz T and Samwer K 1966 *Thin Solid Films* **275** 176
[17] Otto T, Stobiecki T, Stobiecki F and Röll K 1993 *J. Magn. Magn. Mater.* **101** 207
[18] Clemens B M and Hufnagel T C 1993 *J. Alloys Compounds* **194** 221
[19] Ryan D H, Coey J M D, Batalla E, Altounian Z and Ström-Olsen J O 1987 *Phys. Rev.* B **35** 8630
[20] Unruh K M and Chien C L 1984 *Phys. Rev.* B **30** 4968

[21] Altounian Z, Shank R J and Ström-Olsen J O 1985 *J. Appl. Phys.* **58** 1192
[22] Paesano A, Teixeira S R and Amaral L 1994 *Hyperfine Interact.* **83** 333
[23] Kopcewicz M and Williamson D L 1993 *J. Appl. Phys.* **74** 4363
[24] Kopcewicz M, Jagielski J, Stobiecki T, Stobiecki F and Gawlik G 1994 *J. Appl. Phys.* **76** 5232
[25] Castaño F J, Stobiecki T, Gibbs M R J and Blythe H J 1997 *J. Phys.: Condens. Matter* **9** 1609
[26] Zhou Xiao-Min and Chen Sow-Hsin 1995 *Phys. Rep.* **257** 223
[27] Hesse J and Rübartsch A 1974 *J. Phys. E: Sci. Instrum.* **7** 526
[28] LeCaer G and Dubois J M 1979 *J. Phys. E: Sci. Instrum.* **12** 1083
[29] Arrot A and Noakes J E 1967 *Phys. Rev. Lett.* **19** 786
[30] Warren B E 1969 *X-ray Diffraction* (Reading, MA: Addison-Wesley) p 253
[31] Hollanders M A, Thijsse B J and Mittemeijar E J 1990 *Phys. Rev.* B **42** 5481
[32] Gibaud A, Cowley R A, McMorrow D F, Ward R C C and Wells M R 1993 *Phys. Rev.* B **48** 14 463
[33] Landes J, Sauer C, Kabius B and Zinn W 1991 *Phys. Rev.* B **44** 8342
[34] Jacobs I S and Bean C P *Fine particles, Thin Films and Exchange Anisotropy (Effects of Finite Dimensions and Interfaces on Basic Properties of Ferromagnets) (Springer Series in Solid-State Sciences)* (Berlin: Springer)
[35] Kossacki P, Stobiecki T and Szymczak H 1993 *Acta Phys. Pol.* A **83** 785
[36] Ausloos M and Elliott R J (eds) 1983 *Magnetic Phase Transitions (Springer Series in Solid-State Sciences)* (Berlin: Springer) p 237
[37] Krebs H U, Webb D J and Marshall A F 1987 *Phys. Rev.* B **35** 5392
[38] Xiao Gang and Chien C L 1987 *J. Appl. Phys.* **61** 3246